

The origin of MOND acceleration and deep-MOND behavior from mass and energy cascade in dark matter flow

Zhijie (Jay) Xu^{1*}

¹Physical and Computational Sciences Directorate, Pacific Northwest National Laboratory; Richland, WA 99352, USA

*Email: zhijie.xu@pnnl.gov, zhijiexu@hotmail.com

Abstract:

The MOND paradigm is an empirically motivated theory with modified gravity to reproduce many astronomical observations without invoking the dark matter hypothesis. Instead of falsifying the existence of dark matter, we propose that MOND is an effective theory naturally emerging from the long-range interaction and collisionless nature of dark matter flow. It essentially describes the dynamics of baryonic mass suspended in fluctuating dark matter fluid. We first review the unique properties of self-gravitating collisionless dark matter flow (SG-CFD), followed by their implications in the origin of MOND theory. To maximize system entropy, the long-range interaction requires a broad size of halos to be formed. These halos facilitate an inverse mass and energy cascade from small to large mass scales that involves a constant rate of energy transfer $\varepsilon_u \approx -4.6 \times 10^{-7} m^2/s^3$ across different scales. In addition to the velocity fluctuation with a typical scale u , the long-range interaction leads to a fluctuation in acceleration with a typical scale a_0 that matches the value of critical MOND acceleration. The velocity and acceleration fluctuations in dark matter flow satisfy the equality $\varepsilon_u = -a_0 u / (3\pi)^2$ that determines the critical MOND acceleration. A notable (unexplained) coincidence of cosmological constant $\Lambda \propto (a_0/c)^2$ might point to a dark energy density proportional to the variance of acceleration fluctuation, i.e. $\rho_{vac} \propto a_0^2/G$. With $u_0 \equiv u(z=0) \approx 354.61 \text{ km/s}$ from N-body simulation, the value of $a_0(z=0) \approx 1.2 \times 10^{-10} m/s^2$ can be obtained. The mass and energy cascade represents an intermediate statistically steady state of dark matter flow. For a given particle velocity v_p , the maximum entropy distributions developed from mass/energy cascade lead to a particle kinetic energy $\varepsilon_k \propto v_p$ at small acceleration $a < a_0$ and $\varepsilon_k \propto v_p^2$ for $a > a_0$. Combining this with the constant rate of energy transfer ε_u , both regular Newtonian dynamics and “deep-MOND” behavior can be fully recovered.

One-Sentence Summary:

The nature of self-gravitating collisionless dark matter flow might reveal the origin of MOND theory.

Contents

INTRODUCTION	3
RESULTS.....	4
<i>N-body simulations for dark matter flow.....</i>	<i>4</i>
<i>Energy cascade in dark matter flow.....</i>	<i>5</i>
<i>The maximum entropy distributions in dark matter flow.....</i>	<i>6</i>
<i>Distributions of acceleration in dark matter flow</i>	<i>8</i>
<i>The origin of critical MOND acceleration and deep-MOND behavior</i>	<i>13</i>
CONCLUSION	17
References and Notes.....	19

INTRODUCTION

The most intriguing mystery of modern astrophysics is the dark matter problem, which originates from the discrepancies between required amount of mass by the astronomical observations and the directly observed amount of luminous mass. A striking example comes from the dynamical motions of astronomical objects. The flat rotation curves of spiral galaxies directly point to the discrepancy in mass: the total mass predicted from the Newtonian gravity is much greater than the observed mass from luminous matter [1, 2]. The standard cosmological model (Λ CDM) interprets this mass discrepancy in terms of the cold dark matter (CDM). Though the nature of dark matter is still unclear, it is widely believed that dark matter is cold (non-relativistic), collisionless, dissipationless (optically dark), non-baryonic, and barely interacting with baryonic matter except through gravity. In addition, dark matter (DM) must be sufficiently smooth on large scales with a fluid-like behavior. However, no conclusive signals have been detected in either direct or indirect searches of DM.

An alternative interpretation resorts to the modification of our understanding of gravity that might eliminate the need of dark matter. The modified gravity must reproduce all astronomical observations (flat rotation curve etc.) with only the observed baryonic mass distribution. In 1977, Tully and Fisher established an empirical relation for rotation curves of galaxies with a wide range of masses M [3], where the flat rotation velocity $v_f \propto M^{1/4}$ or $v_f^4 = GMa_0$. Here G is the gravitational constant and a_0 is an empirical constant of acceleration. The similar scaling was also identified for the velocity dispersion σ for random motion of stars [4], i.e. $\sigma \propto M^{1/4}$. The original modified Newtonian Dynamics (MOND) is a popular empirical model proposed to reproduce these astronomical observations without invoking the dark matter hypothesis [5]. Further developments were accomplished for the completeness of MOND. Some examples are the relativistic MOND [6, 7]. The basic idea of MOND is to introduce a critical scale of acceleration $a_0 \approx 1.2 \times 10^{-10} \text{ m/s}^2$. The standard Newtonian mechanics $F = ma$ is recovered when acceleration $a \gg a_0$. While for “deep-MOND” regime where $a \ll a_0$, Newtonian mechanics should be modified to $F = ma^2/a_0$, i.e. the external force $F \propto a^2$. As an ad hoc empirically motivated theory, MOND successfully explains the shape of rotation curves [8], the baryonic Tully-Fisher relation [9, 10], and many other phenomena on galactic scale. This motivates the search of a fundamental theory explaining the MOND paradigm.

In conventional wisdom, MOND is a competing empirical theory that potentially falsifies the dark matter hypothesis. In this paper, we propose that MOND is essentially an intrinsic feature of and consistent with dark matter flow. Instead of falsifying the existence of dark matter, MOND is an effective theory describing the dynamics of baryonic mass suspended in dark matter fluid, which mimics the Brownian motion. To explain this, we need to understand the nature of self-gravitating collisionless fluid dynamics (SG-CFD) for dark matter flow. At first glance, both SG-CFD and regular hydrodynamic turbulence contain same features including the randomness, nonlinearity, and multiscale nature. The homogeneous isotropic incompressible turbulence has been studied for many decades [11-14]. Turbulence consists of eddies (the building blocks of turbulence) that are interacting with each other. The classical picture of turbulence is an eddy-mediated cascade process. Kinetic energy of large eddies feeds smaller eddies, which feeds even smaller eddies, and so on to the smallest scale when viscous dissipation becomes dominant. There exists a range of length scales with a scale-independent constant rate ε (unit: m^2/s^3) of energy

passing down the cascade. This is the inertial range where the viscous force is negligible and inertial force is dominant. This process (a direct energy cascade) can be described by a poem [15]:

Big whirls have little whirls, That feed on their velocity;
And little whirls have lesser whirls, And so on to viscosity.

While direct energy cascade is a dominant feature for 3D turbulence, there exists a range of scales over which kinetic energy is transferred from small to large length scales in 2D turbulence, i.e. an inverse energy cascade [16]. By comparing with hydrodynamic turbulence, the dark matter flow exhibits following unique behaviors due to its collisionless and long-range interaction nature:

- i) The long-range gravity requires a broad size of halos to be formed to maximize system entropy [17]. Just like the Maxwell-Boltzmann distribution in kinetic theory of gases, maximum entropy distributions for velocity and energy can be analytically derived for SG-CFD [17]. The linear scaling between particle energy and velocity at small acceleration can be essential to understand the “deep MOND” behavior.
- ii) Halos are the building blocks of SG-CFD (counterpart to “eddies” in turbulence) and facilitate an inverse mass cascade from small to large mass scales that is absent in hydrodynamic turbulence. This leads to many new understandings of halo mass function and internal structure (density profiles etc.) in terms of the random-walk of halos in mass space [18, 19].
- iii) Both types of flow are non-equilibrium systems involving energy cascade across different scales [17, 20]. The mass/energy cascade is essentially an intermediate statistically steady state of non-equilibrium systems to continuously maximize system entropy while evolving toward the limiting equilibrium. The baryonic-to-halo mass relation can be analytically derived from the energy cascade [21].
- iv) In addition to the velocity fluctuation, the long-range interaction in dark matter flow also leads to fluctuations in acceleration that might explain the critical MOND acceleration a_0 [22]. By contrast, in kinetic theory of gases, molecules undergo short-range elastic collisions with velocity fluctuation following Maxwell-Boltzmann distribution to maximize system entropy, while acceleration fluctuation is not present.
- v) The viscous force is not present in collisionless dark matter flow. Without viscous force, there is no dissipation in SG-CFD and the smallest length scale of inertial range is not limited by viscosity. This enables us to extend the scale-independent constant energy flux ε down to the smallest scales where quantum effects become important, and predict dark matter particle mass, size and other relevant properties [23].
- vi) Unlike hydrodynamic turbulence that is incompressible on all scales, dark matter flow exhibits scale-dependent flow behaviors, i.e. an incompressible flow for proper velocity (or constant divergence flow for peculiar velocity) on small scales and an irrotational flow on large scales [24-26]. Physical laws, such as the two-thirds law for pairwise velocity dispersion, holds for dark matter flow such that we can apply to identify dark matter particle properties [23].

In this paper, we first review the key properties of dark matter flow, followed by the origin of critical MOND acceleration and the “deep-MOND” behavior based on these properties.

RESULTS

N-body simulations for dark matter flow

The basic dynamics of dark matter flow is governed by the collisionless Boltzmann equations (CBE) [27] that can be numerically solved by particle-based N-body simulations [28]. The simulation data for this work was generated from large scale N-body simulations by the Virgo

consortium [29, 30]. The current work focuses on the matter-dominant simulations with $\Omega_0 = 1$ and cosmological constant $\Lambda = 0$. The same set of simulation data has been widely used in various studies such as the clustering statistics [30], the formation of halo clusters in large scale environments [31], and testing models for halo abundance and mass functions [32]. Key parameters of N-body simulations are listed in Table 1, where h is the Hubble constant in the unit of $100 \text{ km}/(\text{Mpc} \cdot \text{s})$, N is the number of particles, and m_p is the particle mass.

Table 1. Numerical parameters of N -body simulation for SCDM

Run	Ω_0	Λ	h	Γ	σ_8	$L(\text{Mpc}/h)$	N	$m_p (M_{\text{sun}}/h)$	$l_{\text{soft}} (\text{Kpc}/h)$
SCDM1	1.0	0.0	0.5	0.5	0.51	239.5	256^3	2.27×10^{11}	36

The friends-of-friends algorithm (FOF) was used to identify all halos in simulation that depends only on a dimensionless parameter b , which defines the linking length $b(N/V)^{-1/3}$, where V is the volume of simulation box. All halos in simulation were identified with a linking length parameter of $b = 0.2$ in this work. All halos identified were grouped into halo groups of different size according to halo mass m_h (or n_p , the number of particles in each halo), where $m_h = n_p m_p$. The total mass for a group of halos of mass m_h is $m_g = m_h n_h$, where n_h is the number of halos in that group. A halo-based non-projection approach is applied to perform the statistical analysis in this paper [22]: i) all halos were identified with all particles divided into halo and out-of-halo particles; ii) instead of projecting particle field onto structured grid that involves information loss, a ‘‘pairwise’’ statistical analysis can be performed over all particle pairs with a given separation r . Simulation results are presented to describe the mass/energy cascade across halo groups of different mass scales.

Energy cascade in dark matter flow

The rate of energy transfer ε_u can be obtained from the formulation of mass/energy cascade [20, 21]. Alternatively, it can be obtained from the energy evolution of entire self-gravitating collisionless system that can be described by a cosmic energy equation (Irvine and Layzer [33, 34] and reformulated in [35]),

$$\frac{\partial E_y}{\partial t} + H(2K_p + P_y) = 0. \quad (1)$$

This equation is a manifestation of energy conservation in expanding background. Here K_p is the specific (peculiar) kinetic energy, P_y is specific potential energy in physical coordinate, $E_y = K_p + P_y$ is total specific energy, and $H = \dot{a}/a$ is the Hubble parameter. The cosmic energy equation (1) admits a power-law solution of $K_p \propto t$ and $P_y \propto t$ (see Fig. 1) such that a constant rate of energy production ε_u can be defined from $K_p = -\varepsilon_u t$ and estimated as [20, 35, 36]

$$\varepsilon_u = -\frac{K_p}{t} = -\frac{3 u^2}{2 t} = -\frac{3 u_0^2}{2 t_0} = -\frac{9}{4} H_0 u_0^2 \approx -4.6 \times 10^{-7} \frac{m^2}{s^3}, \quad (2)$$

where $u_0 \equiv u(t = t_0) \approx 354.61 \text{ km}/s$ is the one-dimensional velocity dispersion of dark matter flow in N-body simulation.

The proportional constant ε_u has a profound physical meaning as the rate of energy cascade across different mass scales [20] that is facilitated by the inverse mass/energy cascade [19]. The negative value $\varepsilon_u < 0$ reflects the inverse energy cascade. The constant ε_u is a fundamental quantity that determines the critical MOND acceleration, i.e. $a_0 = (3\pi)^2 (-\varepsilon_u/u) \approx 1.2 \times 10^{-10} \text{ m/s}^2$ (see Eq. (14)). In addition, for collisionless dark matter flow with gravity being the only interaction involved, the absence of viscosity enables us to extend the scale-independent energy cascade down to the smallest scale where quantum effects are dominant. Combining the energy flux ε_u , Planck constant \hbar , and gravitational constant G on the smallest scale, the mass of dark matter particles can be predicted to be around $m_\chi \approx 0.9 \times 10^{12} \text{ GeV}$ with a size on the order of $3.1 \times 10^{-13} \text{ m}$ [23].

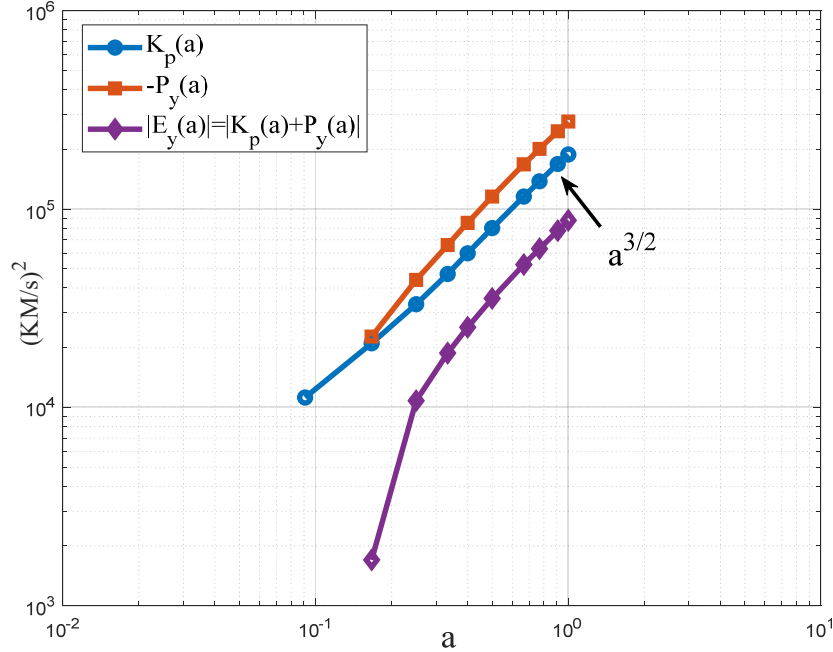


Figure 1. The time variation of specific kinetic and potential energies from N -body simulation. Both energies exhibit power-law scaling with the scale factor a , i.e. $K_p(a) = -\varepsilon_u t \propto a^{3/2} \propto t$ and $P_y(a) \propto a^{3/2} \propto t$. The proportional constant ε_u is the rate of energy transfer that is estimated in Eq. (2).

The maximum entropy distributions in dark matter flow

The halo-mediated mass/energy cascade is an intermediate statistically steady state of non-equilibrium dark matter flow to continuously maximize system entropy while evolving towards the limiting equilibrium. In the kinetic theory of gases, the Boltzmann distribution is the maximum entropy distribution for velocity in equilibrium. In dark matter flow (SG-CFD), the maximum entropy distributions of DM particle velocity, speed, and energy are also gradually developed through continuous mass/energy cascade [17]. For system with long-range interaction and gravitational potential $V(r) \propto r^n$ (exponent $-2 < n < 0$), a broad size of halos is required to be formed to maximize the system entropy [17]. Applying the virial equilibrium for mechanical equilibrium in halo groups, and the maximum entropy principle for statistical equilibrium of global system, maximum entropy distributions can be analytically derived. The halo mass function can be

subsequently derived as a direct result of entropy maximization [37]. The maximum entropy velocity distribution (the X -distribution) involves a shape parameter α and a velocity scale v_0 [17],

$$X(v) = \frac{1}{2\alpha v_0} \frac{e^{-\sqrt{\alpha^2 + (v/v_0)^2}}}{K_1(\alpha)}, \quad (3)$$

where $K_y(x)$ is a modified Bessel function of *second kind*. Parameter α dominates the shape of X distribution. The X distribution approaches a double-sided Laplace (exponential) distribution with $\alpha \rightarrow 0$ and a Gaussian distribution with $\alpha \rightarrow \infty$, respectively. For intermediate α , the X distribution naturally exhibits a Gaussian core at small velocity $v \ll v_0$ and exponential wings at large velocity $v \gg v_0$ (see Fig. 2) [17]. In Fig. 2, the longitudinal velocity u_L is computed as the projection of particle velocity \mathbf{u} along the direction of the separation \mathbf{r} of a pair of particles, i.e. $u_L = \mathbf{u} \cdot \mathbf{r}$. Particle velocity is normalized by σ_0^2 to have a unit variance. Here distribution parameters $\alpha = 1.33$, $v_0^2 = 1/3 \sigma_0^2$, and $\sigma_0^2 = \text{var}(u_L)$ on the scale of $r \equiv |\mathbf{r}| = 0.1 \text{ Mpc}/h$. The scale and redshift dependence of velocity distributions in dark matter flow are extensively studied in [22] using a halo-based non-projection approach. In this paper, a similar approach is also applied to study the acceleration distributions in dark matter flow.

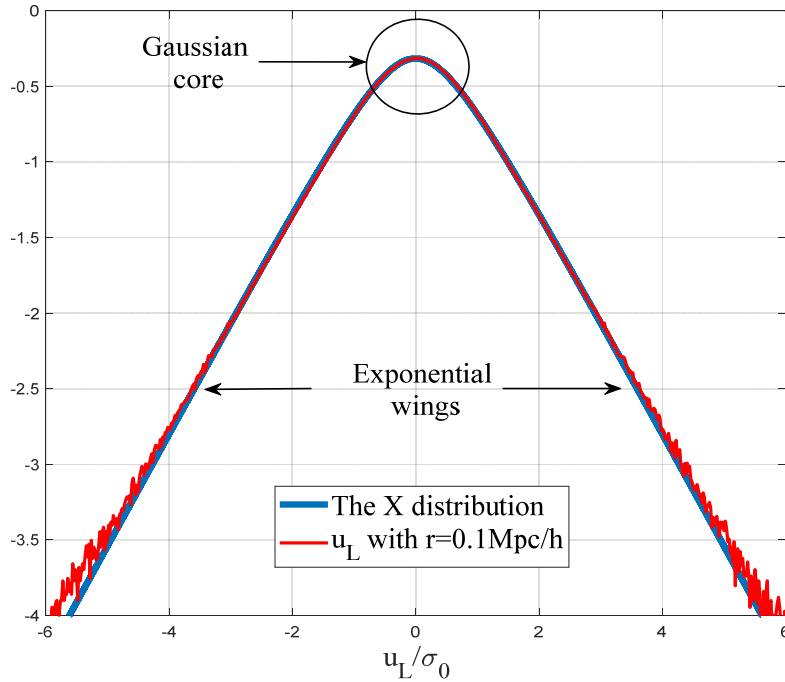


Figure 2. The X distribution with a unit variance compared with the velocity distribution from N -body simulation (u_L normalized by σ_0). Vertical axis is in the logarithmic scale (\log_{10}). The X distribution with $\alpha = 1.33$ and $v_0^2 = 1/3 \sigma_0^2$ matches the velocity distribution of small r , where all pairs of particles are likely from the same halo. The Gaussian core ($u_L < v_0$) and exponential wings ($u_L > v_0$) can be clearly identified.

Finally, the specific particle energy $\varepsilon(v)$ for DM particles with a given speed $v \equiv |\mathbf{v}|$ can be obtained from maximum entropy distributions [17]. We have the particle energy $\varepsilon(v)$,

$$\varepsilon(v) = \frac{3}{2} \left(1 + \frac{2}{n}\right) v_0^2 \sqrt{\alpha^2 + \left(\frac{v}{v_0}\right)^2}, \quad (4)$$

where $\varepsilon(v)$ follows a linear scaling for large velocity and a parabolic scaling for small velocity,

$$\begin{aligned} \varepsilon(v) &\approx \frac{3}{2} \left(1 + \frac{2}{n}\right) v_0 v && \text{for } v \gg v_0, \\ \varepsilon(v) &\approx \frac{3}{2} \left(1 + \frac{2}{n}\right) \left(\alpha v_0^2 + \frac{v^2}{2\alpha}\right) && \text{for } v \ll v_0, \end{aligned} \quad (5)$$

where n is the potential exponent. Specific energy $\varepsilon(v)$ includes both kinetic and potential energy. Using virial theorem, the specific kinetic energy for particles with a given speed $|\mathbf{v}|$ should also follow $\varepsilon_K(v) \propto |\mathbf{v}|^2$ for low-speed ($|\mathbf{v}| \ll v_0$), which is the standard Newtonian behavior. However, $\varepsilon_K(v) \propto v_0 |\mathbf{v}|$ for high-speed particles ($|\mathbf{v}| \gg v_0$) is unique for dark matter flow. The kinetic energy proportional to particle velocity might be a manifestation of the external field effect that is often discussed in MOND literature. These high-speed particles are usually in the outer region of halos with extremely small acceleration. Their dynamics is much easier to be affected by the presence of external gravitational field (inter-halo interaction with other halos) due to the long-range nature of gravity. The superimposition of all intra- and inter-halo interactions leads to this linear scaling, which also emerges from maximizing system entropy. This scaling is critical for understanding the “deep-MOND” behavior.

Distributions of acceleration in dark matter flow

The density and velocity distributions were extensively studied for dark matter flow in [22]. In kinetic theory of gases, molecules undergo random elastic collisions with a short-range of interaction. Particle acceleration also vanishes because of the short-range interaction and fluctuation of acceleration is not present. By contrast, the long-range gravity in dark matter flow inevitably leads to fluctuations in particle acceleration, in addition to the fluctuation in velocity. This unique feature hints to the potential generalization of standard Brownian/Langevin dynamics to include acceleration fluctuation for dark matter flow. There can be tremendous amount of work to explore along this direction. In this paper, the distribution of acceleration is explicitly studied to demonstrate that the critical MOND acceleration a_0 can be related to the fluctuation of DM particle acceleration. By computing the total force, the proper acceleration for particle i is

$$\mathbf{a}_p = \frac{Gm_p}{a^2} \sum_{j \neq i}^N \frac{\mathbf{x}_i - \mathbf{x}_j}{|\mathbf{x}_i - \mathbf{x}_j|^3}, \quad (6)$$

where \mathbf{x}_i and \mathbf{x}_j are the comoving spatial coordinates of particles i and j . Summation is running over all other particles except i . Periodic boundary is also applied for force calculation with a total of 26 repeats of simulation domain in three-dimension. Figure 3 plots the redshift variation of acceleration distribution, i.e. the distribution of Cartesian component $[a_{px}, a_{py}, a_{pz}]$ of acceleration

vector \mathbf{a}_p for all particles. The particle acceleration evolves from an initial Gaussian distribution at high redshift to a distribution with a long tail $\propto a_p^{-3}$ for large acceleration in halo core region. Tail starts to form at around $z=5$ due to the formation of halos.

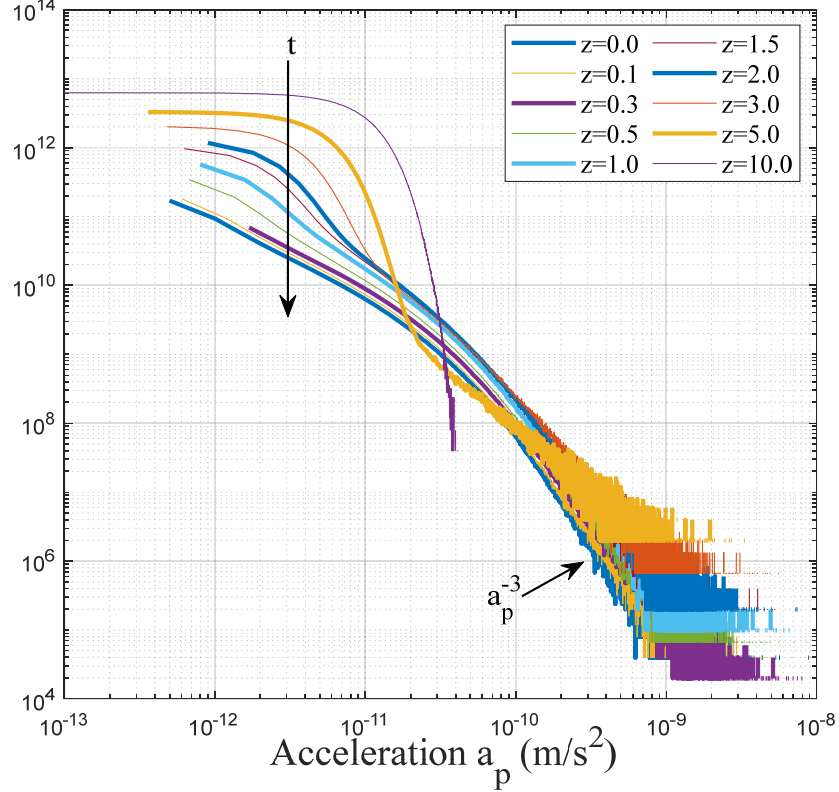


Figure 3. The redshift evolution of the distribution of particle acceleration a_p . A long tail $\propto a_p^{-3}$ is gradually formed from $z=5$ due to the formation of halo structures.

Just like the halo-based non-projection approach for velocity distributions [22], we identify all halos in N-body system and divide all DM particles into halo and out-of-halo particles since distributions are evolving differently for different types of particles. Figure 4 plots the redshift evolution of distributions of a_{hp} for halo particles (solid lines) and a_{op} for out-of-halo particles (dash lines). The long tail $\propto a_{hp}^{-3}$ at large acceleration comes from halo core region with higher density. The maximum particle acceleration is determined by the highest density at halo core and is independent of the redshift. With inverse mass cascade [19], more particles are accreted into the halo outer region and the distribution gradually extends to smaller acceleration. The distribution of a_{op} for out-of-halo particles is relatively Gaussian for all redshifts. Acceleration decreases with time due to the expanding space (Fig. 5). The out-of-halo particles with the greatest acceleration should be from particles close to the surface of halos that they are merge with (red arrow). More study should be pursued on the analytical models of acceleration distribution.

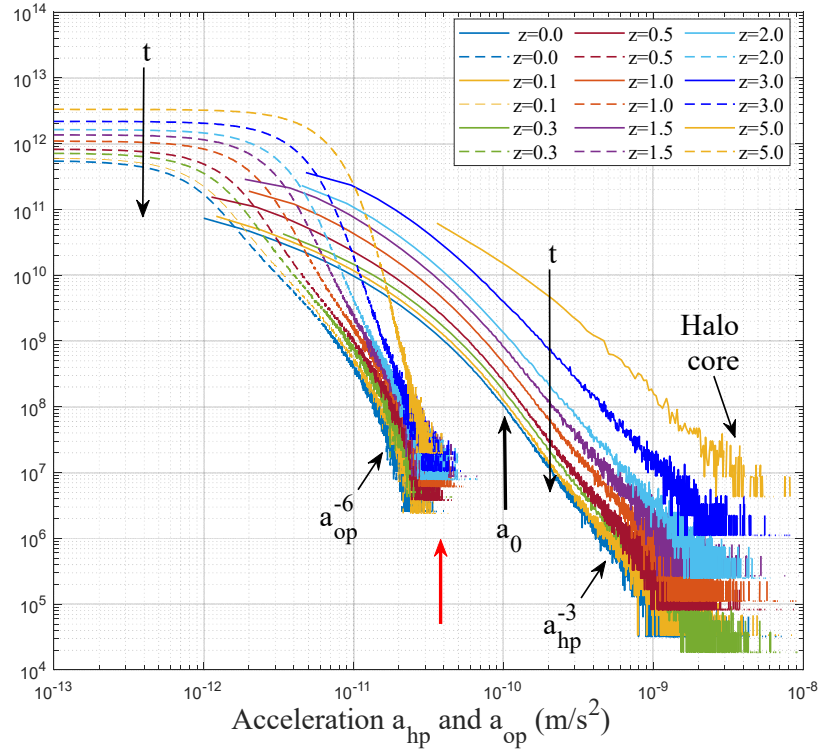


Figure 4. The redshift evolution of halo particle acceleration a_{hp} (solid lines) and out-of-halo particle acceleration a_{op} (dash lines). A long tail $\propto a_{hp}^{-3}$ at large acceleration is a typical feature from halo particles in core region. The distribution of a_{op} for out-of-halo particles is relatively Gaussian. For both types of particles, acceleration decreases with time (Fig. 5). Critical MOND acceleration ($a_0 \approx 10^{-10} m/s^2$) is marked in the plot (black arrow).

Figure 5 plots the time variation of typical accelerations ($\sqrt{3} \times$ standard deviation of distributions in Figs. 3 and 4, i.e. the root-mean-square acceleration) for all particles (blue), halo particles (black), out-of-halo particles (red), and halos (green), where the factor $\sqrt{3}$ is for the magnitude of acceleration vector in 3D space. The halo acceleration a_h is the mean acceleration of all particles in the same halo. All typical accelerations decrease with time (approximately $\propto a^{-3/4}$ for halo particles and $\propto a^{-1/2}$ for out-of-halo particles and halos). The only exception is the halo particle acceleration at $z=0.3$ (red circle) that is greater than acceleration at both $z=0.5$ and $z=0.1$ that requires further confirmation from other N-body simulations. On large scale, halos and out-of-halo particles have similar accelerations that are much smaller than the acceleration of halo particles due to greater distance ($\sim 10^{-12} m/s^2$, green and red lines). At $z=0$, the typical acceleration of halo particles matches the critical MOND acceleration, where $a_0 = 1.2 \times 10^{-10} m/s^2$.

Similarly, Figure 6 plots the variation of velocity variance with scale factor a . The variance of halo velocity v_h matches the out-of-halo particle velocity v_{op} with a scaling $\propto a$. The variance of all particles is dominated by out-of-halo particles at early time ($\langle v_p^2 \rangle \propto a$) and transition to $\langle v_p^2 \rangle \propto a^{3/2}$ at a late time (dominated by halo particle velocity).

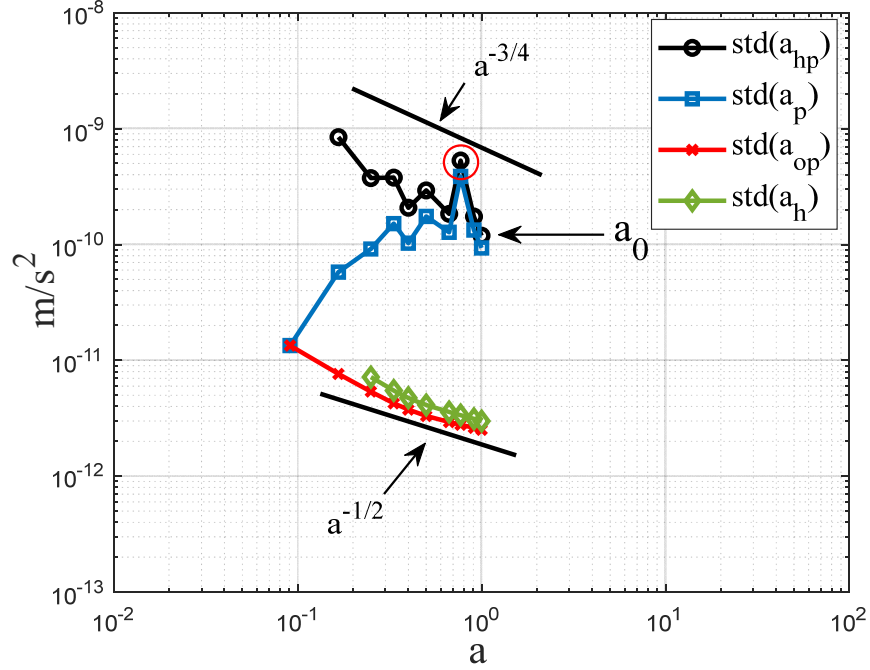


Figure 5. The variation of typical (root-mean-square) accelerations with scale factor a for all particles (a_p : blue), halo particles (a_{hp} : black), out-of-halo particles (a_{op} : red), and halos (a_h : green), respectively. All Accelerations decrease with time. At $z=0$, the typical acceleration of halo particles matches the critical MOND acceleration $a_0 = 1.2 \times 10^{-10} \text{ m/s}^2$. The halo acceleration a_h matches the out-of-halo particle acceleration a_{op} and is much smaller ($\sim 10^{-12} \text{ m/s}^2$) due to weaker gravity on large scale.

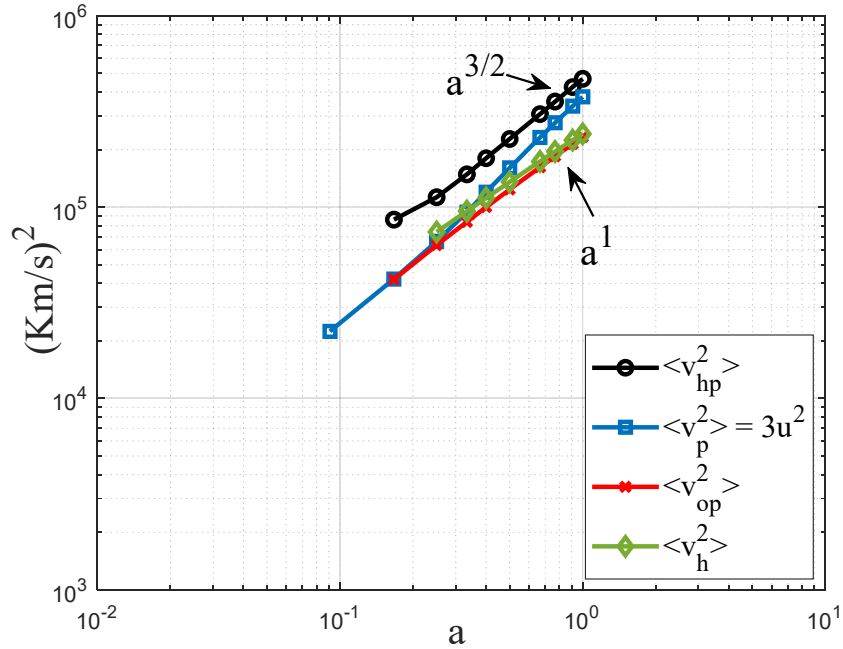


Figure 6. The variation of velocity variance with scale factor a for all particles (v_p : blue), halo particles (v_{hp} : black), out-of-halo particles (v_{op} : red), and halos (v_h : green), respectively. All velocity variances increase with time. The variance of halo velocity v_h matches the out-of-halo particle velocity v_{op} with a scaling $\propto a$. The variance of all particles (blue) is dominated by out-of-halo particles at early time ($\langle v_p^2 \rangle \propto a$) and transition to $\langle v_p^2 \rangle \propto a^{3/2}$ at a late time (dominated by halo particle velocity).

We next identify all halos in N-body system and group halos according to their size n_p (the number of particles in halo) or halo mass $m_h = n_p m_p$. For every halo, the acceleration \mathbf{a}_{hp} and velocity \mathbf{v}_{hp} of halo particles can be further decomposed into the contribution due to intra-halo interaction,

$$\mathbf{a}_{hp}^i = \mathbf{a}_{hp} - \langle \mathbf{a}_{hp} \rangle_h = \mathbf{a}_{hp} - \mathbf{a}_h \quad \text{and} \quad \mathbf{v}_{hp}^i = \mathbf{v}_{hp} - \langle \mathbf{v}_{hp} \rangle_h = \mathbf{v}_{hp} - \mathbf{v}_h, \quad (7)$$

and the contribution due to inter-halo interaction (i.e. the halo acceleration and velocity),

$$\mathbf{a}_h = \langle \mathbf{a}_{hp} \rangle_h = \frac{1}{n_p} \sum_{k=1}^{n_p} \mathbf{a}_{hp} \quad \text{and} \quad \mathbf{v}_h = \langle \mathbf{v}_{hp} \rangle_h = \frac{1}{n_p} \sum_{k=1}^{n_p} \mathbf{v}_{hp}, \quad (8)$$

where $\langle \cdot \rangle_h$ stands for the average a quantity over all particles in a given halo. On halo level, the typical acceleration in each halo a_h^i can be computed as the root-mean-square of intra-halo particle acceleration \mathbf{a}_{hp}^i for all particles in the same halo, i.e. $a_h^i = \left\langle |\mathbf{a}_{hp}^i|^2 \right\rangle_h^{1/2}$. The halo acceleration \mathbf{a}_h is the mean acceleration of all particles in the same halo, i.e. $\mathbf{a}_h = \langle \mathbf{a}_{hp} \rangle_h$ in Eq. (8).

On group level (a group of all halos with the same size n_p), the typical acceleration in halo (a_{hg}^i) can be computed as the mean intra-halo acceleration a_h^i of all halos in the same group, i.e. $a_{hg}^i = \langle a_h^i \rangle_g$, where $\langle \cdot \rangle_g$ stands for average over all halos in the same group. The typical halo acceleration a_{hg} can be computed as the root-mean-square of halo acceleration \mathbf{a}_h for all halos in the same group, i.e. $a_{hg} = \left\langle |\mathbf{a}_h|^2 \right\rangle_g^{1/2}$. Similar statistics were also applied to particle velocity \mathbf{v}_{hp} to obtain the halo virial dispersion σ_v^2 and halo velocity dispersion σ_h^2 (see [20]).

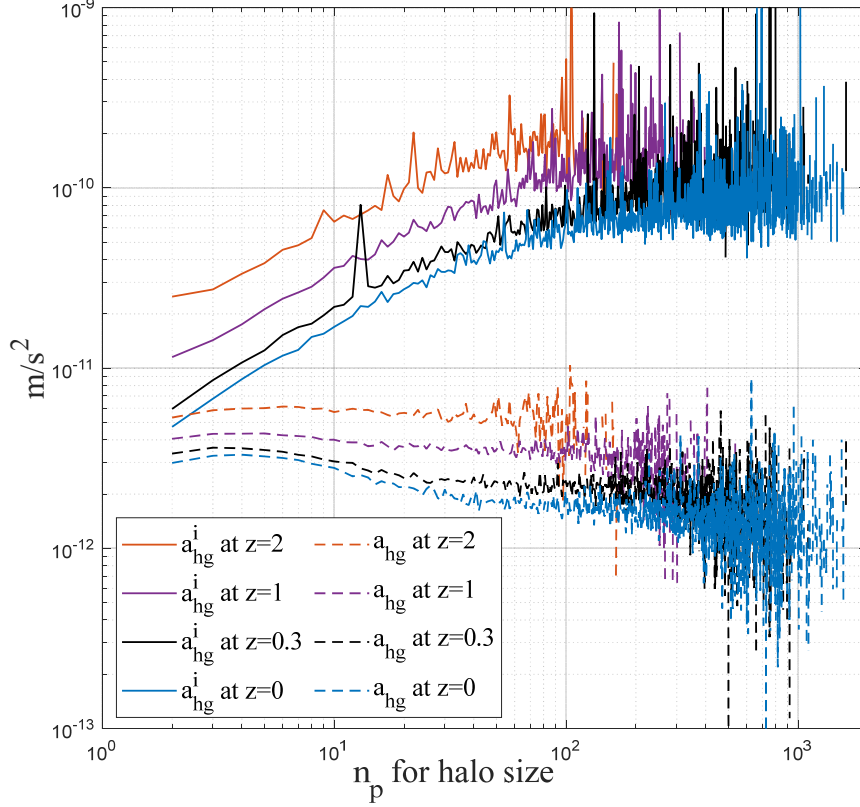


Figure 7. The variation of typical acceleration in halos (a_{hg}^i : solid lines) and acceleration of halos (a_{hg} : dash lines) with halo size n_p at different redshifts z . Halo mass $m_h = n_p m_p$. Both accelerations decrease with time at a given halo size, while acceleration in halos increases with halo size (roughly $a_{hg}^i \propto (m_h)^{2/3} a^{-1}$ for small n_p and $a_{hg}^i \propto (m_h)^{1/3} a^{-1}$ for large n_p) and reaches about $10^{-10} m/s^2$ for large halos. Acceleration of halos a_{hg} is independent of halo size n_p , much smaller and on the order of $10^{-12} m/s^2$.

Figure 7 plots the variation of typical accelerations in halos (a_{hg}^i : solid lines) and acceleration of halos (a_{hg} : dash lines) with halo size n_p at different redshifts z . Halo mass $m_h = n_p m_p$ with $m_p = 2.27 \times 10^{11} M_\odot/h$. For same halo size n_p , both accelerations decrease with time. Acceleration in halos a_{hg}^i increases with halo size and reaches about $10^{-10} m/s^2$ for large halos. Acceleration of halos a_{hg} is relatively independent of halo size, much smaller than acceleration in halos and roughly on the order of $10^{-12} m/s^2$ due to weaker gravity between halos on large scale.

The origin of critical MOND acceleration and deep-MOND behavior

Note that the typical acceleration in halos (a_{hp} in Fig. 5) at $z=0$ matches the critical MOND acceleration $a_0 = 1.2 \times 10^{-10} m/s^2$ [5], which hints a_0 might be an intrinsic property of dark matter

flow due to the fluctuation of acceleration. The value of a_0 is still empirical and phenomenological without a good theory. A brief estimation of the critical acceleration a_0 can be made here based on the inverse mass/energy cascade in dark matter flow [19, 20].

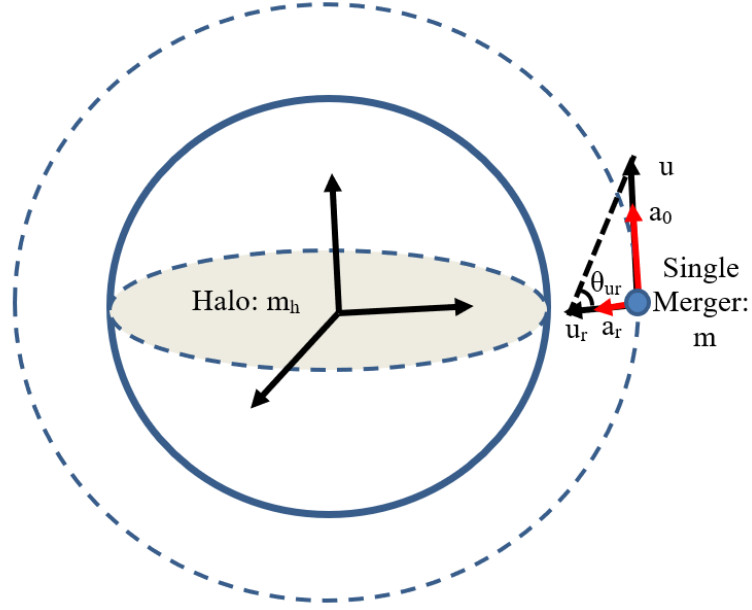


Figure 8. The schematic plot for inverse mass/energy cascade from a series of merging between halo and single mergers. For an infinitesimal interval dt , that process should only involve the merging of a halo (mass: m_h) with a single merger (mass: m). The single merger has a typical velocity $u(a)$ (black) and a typical acceleration $a_0(a)$ (red). Dash line represents the boundary of that halo.

In a finite time interval Δt , the hierarchical structure merging might involve multiple substructures merging into a single large structure. For an infinitesimal time interval dt , that process should involve the merging of two and only two substructures (see Fig. 8) such that the two-body collapse is the most elementary process for halo mass accretion and inverse mass cascade [36]. The consecutive elementary merging between a halo and a single merger facilitates the inverse mass and energy cascade [19, 20]. Let's consider a two-body merging, where a single merger has a mass m , a typical velocity $u(a)$ from velocity fluctuation, and a typical acceleration $a_0(a)$ from acceleration fluctuation, right before the merging with a halo of mass m_h . The velocity and acceleration of single merger are likely aligned on large scale (velocity \mathbf{u} and acceleration \mathbf{a}_0 point to the same direction). Due to the gravitational interaction with halo to be merged, the single merger right on the boundary (dash line) has a relative motion toward the center of halo $u_r = u \cot(\theta_{ur})$ (the radial velocity) and a radial acceleration toward halo center with $a_r = a_0 \cot(\theta_{ur})$. The angle θ_{ur} can be related to the critical value β_{s2} for an equilibrium two-body collapse (Eq. (104) in [36]), i.e.,

$$\cot(\theta_{ur}) = \frac{u_r}{v_{cir}} = \beta_{s2} = \frac{1}{3\pi}, \quad (9)$$

where v_{cir} is the circular velocity at the surface of halo ($u \approx v_{cir}$). Here β_{s2} is a constant that is related to the critical halo density as $\Delta_c = 2/(\beta_{s2})^2 = 18\pi^2$ (Eq. (89) in [36]). This is also true for isothermal halos where the ratio between circular velocity and radial flow is $v_{cir}/u_r = 3\pi$ (Eq. (29) in [18]). It can also be demonstrated with the radial velocity $u_r = Hr_h = v_{cir}/(3\pi)$. Here

$$m_h = \frac{4}{3}\pi r_h^3 \Delta_c \bar{\rho} \quad \Rightarrow \quad v_{cir} = \frac{Gm_h}{r_h} = Hr_h \sqrt{\frac{\Delta_c}{2}}, \quad (10)$$

where Hubble parameter $H = 8\pi G\bar{\rho}/3$ and $\bar{\rho}(t)$ is the mean matter density.

Now let's try to compute the constant rate of energy cascade in dark matter flow in several different ways. First, that rate (ε_u in m^2/s^3) represents the energy flux/transfer across halos of different mass scales. It can be determined by the change of total kinetic energy of all halo particles due to the intra-halo motion (defined in Eqs. (7) and (8)), i.e. a dot product between \mathbf{a}_{hp}^i and \mathbf{v}_{hp}^i ,

$$\varepsilon_u = -\langle \mathbf{a}_{hp}^i \cdot \mathbf{v}_{hp}^i \rangle = -\langle \mathbf{a}_{hp} \cdot \mathbf{v}_{hp} \rangle + \underbrace{\langle \mathbf{a}_h \cdot \mathbf{v}_h \rangle}_1, \quad (11)$$

where \mathbf{a}_{hp} and \mathbf{v}_{hp} are halo particle acceleration and velocity, while \mathbf{a}_{hp}^i and \mathbf{v}_{hp}^i are particle acceleration and velocity relative to the motion of halos. The average is taken over all halo particles in all halos. Terms \mathbf{a}_h and \mathbf{v}_h are the acceleration and velocity of halos, i.e. the mean acceleration and velocity of all particles in a given halo. The change of kinetic energy due to the motion of halos (term 1 in Eq. (11)) does not contribute to energy cascade and should be excluded.

Second, the inverse mass/energy cascade is facilitated by a series of merging with single mergers [19, 20]. The rate of kinetic energy cascade might be directly determined from a typical merging process, i.e. a two-body collapse model (TBCM model in [36]). During each merging, the kinetic energy transferred from small to large mass scale (from m_h to $m_h + m$) comes from the change of kinetic energy of that single merger at the instant of merging, mostly via the relative motion along radial direction. The motion in tangential direction does not contribute to the energy cascade. For a single merger with a typical velocity $u(a)$ and a typical acceleration $a_0(a)$, the rate of energy transfer ε_u approximately reads

$$\varepsilon_u = -a_r u_r = -a_0(a) \cot(\theta_{ur}) u(a) \cot(\theta_{ur}), \quad (12)$$

where $\varepsilon_u < 0$ for inverse cascade. This expression resembles the first expression in Eq. (11), but is obtained from the elementary two-body merging process.

Third, by considering the energy evolution in entire N-body system, the rate of energy transfer is approximately the change of specific kinetic energy for entire system, or rate of energy production. It is a constant of time (see Fig. 1 and Eq. (2)) and should read

$$\varepsilon_u \approx -\frac{3}{2} \frac{u^2}{t} = -\frac{3}{2} \frac{u_0^2}{t_0} = -\frac{9}{4} H_0 u_0^2 = -4.6 \times 10^{-7} \frac{m^2}{s^3}. \quad (13)$$

Combining Eqs. (9)-(13) together, the typical acceleration $a_0(a)$ can be related to ε_u as

$$a_0(a) = -\frac{\Delta_c}{2} \cdot \frac{\varepsilon_u}{u} = -(3\pi)^2 \frac{\varepsilon_u}{u} = \frac{81}{4} \pi^2 H_0 \frac{u_0^2}{u} \propto a^{-3/4}, \quad (14)$$

where with $u_0 = 354.61 \text{ km/s}$ and $H_0 = 100h \text{ km}/(s \cdot \text{Mpc}) \approx 1.62 \times 10^{-18} \text{ 1/s}$ (with $h = 0.5$),

$$a_0(a=1) \approx 200 H_0 u_0 \approx 1.2 \times 10^{-10} \text{ m/s}^2. \quad (15)$$

The redshift dependence of critical acceleration $a_0(a) \propto a^{-3/4} = (1+z)^{3/4}$ seems consistent with literature that a_0 decreases with scale factor a , but at a slower rate than $a_0(a) \propto a^{-3/2}$ [38, 39].

In addition, with c being the speed of light, Λ being the cosmological constant, and a coincidence pointed out by Milgram [40] that $a_0(z=0) \approx c H_0 / (2\pi) \approx c (\Lambda/3)^{1/2} / (2\pi)$, the constant rate of energy cascade ε_u can be related to c and Λ as (using Eq. (14))

$$\varepsilon_u \approx -\frac{u_0 c H_0}{2\pi (3\pi)^2} \approx -\frac{u_0 c (\Lambda/3)^{1/2}}{2\pi (3\pi)^2},$$

$$\Lambda \approx 3(2\pi)^2 (3\pi)^4 \left(\frac{\varepsilon_u}{u_0 c} \right)^2 = \frac{3(2\pi)^2}{c^2} a_0^2 \approx 2 \times 10^{-35} \frac{1}{s^2}, \quad (16)$$

and the dark energy density reads

$$\rho_{vac} = \frac{\Lambda c^2}{8\pi G} = \frac{3\pi}{2G} \left(\frac{(3\pi)^2 \varepsilon_u}{u_0} \right)^2 = \frac{3\pi}{2} \frac{a_0^2 H_0}{GH}. \quad (17)$$

The exact meaning of this coincidence is not clear and worth to explore. It might indicate some hidden relations between dark energy and the velocity/acceleration fluctuations in dark matter flow ($\rho_{vac} \propto a_0^2$, i.e. the dark energy density is proportional to the variance of acceleration fluctuation).

Finally, we demonstrate that the critical MOND acceleration a_0 can be determined by ε_u (Eq. (14)). Just like the peculiar velocity, there exists a fluctuation of acceleration in dark matter flow. The typical scale of acceleration fluctuation possibly plays the role of the critical MOND acceleration, i.e. the MOND theory might be an intrinsic property of and fully consistent with the theory of dark matter flow. In this regard, instead of falsifying, the MOND theory might indeed support the existence of dark matter.

More insights can be briefly outlined here for the origin of so-called ‘‘deep-MOND’’ behavior, where particle acceleration is much smaller than the fluctuation of acceleration ($|\mathbf{a}_p| \ll a_0$). To simplify the calculation, let’s assume a one-dimensional self-gravitating collisionless fluid with a typical velocity scale v_0 and an acceleration scale a_0 due to the fluctuations of velocity and acceleration. A baryonic particle with mass m_p , velocity v_p , and acceleration $a_p = dv_p/dt$, moves through the collisionless fluid under external force F_p . The driving force F_p can be of any nature including gravity. This is an exact analogue of the Brownian motion with particles suspended in a viscous liquid. To respect the nature of dark matter flow we discussed, the velocity dispersion v_p^2

of that particle should increase linearly with time (Eq. (13)) with a proportional constant $\varepsilon_u = -a_0 v_0$ (θ_{ur} in Eq. (12) does not present for 1D system) such that

$$\frac{1}{2} \frac{dv_p^2}{dt} = v_p \frac{dv_p}{dt} = a_p v_p = a_0 v_0 = -\varepsilon_u. \quad (18)$$

The external force F_p can be computed from the change of specific kinetic energy,

$$F_p v_p = m_p \frac{d\varepsilon_K}{dt}. \quad (19)$$

For “deep-MOND” regime where $a_p \ll a_0$ or $v_p \gg v_0$, the specific kinetic energy $\varepsilon_K(v) = v_0 v_p$ that is proportional to the particle speed v_p (from Eq. (5)). Force in “deep-MOND” regime can be obtained from Eqs. (18) and (19) such that external force $F_p \propto a_p^2$, i.e.

$$F_p = m_p \frac{v_0}{v_p} a_p = m_p \frac{a_p^2}{a_0}. \quad (20)$$

On the other hand, for particles with low speed or high acceleration, i.e. $a_p \gg a_0$ or $v_p \ll v_0$, the specific kinetic energy $\varepsilon_K(v) = v_p^2/2$ such that the standard Newton’s law $F_p = m_p a_p$ can be fully recovered from Eq. (19). Two key ingredients are necessary for this simplistic view of MOND: i) the constant rate of energy cascade for dark matter flow (Eq. (18)); and ii) the kinetic energy proportional to particle speed for low acceleration (Eq. (5)). If both a_0 and v_0 are the standard deviation of acceleration and velocity fluctuation, Eq. (18) represents a new “uncertainty” principle in dark matter flow, such that the more precisely velocity is determined, the less precisely its acceleration can be determined, and vice versa. Future study is required to further refine and develop this simple idea.

CONCLUSION

The main focus of this paper is the study of unique properties of self-gravitating collisionless dark matter flow (SG-CFD) and their implications in the origin of MOND acceleration and “deep-MOND” behavior. In dark matter flow, the long-range interaction requires a broad size of halos to be formed to maximize system entropy. Halos facilitate an inverse mass and energy cascade from small to large mass scales with a constant rate of energy transfer $\varepsilon_u \approx -4.6 \times 10^{-7} m^2/s^3$. The mass/energy cascade represents an intermediate statistically steady state of dark matter flow. The maximum entropy distributions reveal a linear scaling between particle energy and velocity for small particle acceleration. In addition to the velocity fluctuation with a typical scale u , the long-range interaction of dark matter flow also leads to fluctuations in acceleration with a typical scale a_0 . In N-body simulation, the root-mean-square particle acceleration decreases with time and matches the critical MOND acceleration (Fig. 5). The velocity and acceleration fluctuations in dark matter flow satisfy the relation $\varepsilon_u = -a_0 u / (3\pi)^2$ which gives $a_0 \approx 1.2 \times 10^{-10} m/s^2$. MOND turns out to be an effective field theory describing the dynamics of baryonic masses suspended in dark matter flow. Future study can be the potential generalization of Brownian/Langevin dynamics to consider the acceleration fluctuation for dark matter flow. More study should also be explored

on the analytical theory for modeling the distribution of acceleration and the theory to connect dark energy density to fluctuation of acceleration.

References and Notes

1. Rubin, V.C. and W.K. Ford, *Rotation of Andromeda Nebula from a Spectroscopic Survey of Emission Regions*. Astrophysical Journal, 1970. **159**(2): p. 379-&.
2. Rubin, V.C., W.K. Ford, and N. Thonnard, *Rotational Properties of 21-Sc Galaxies with a Large Range of Luminosities and Radii, from Ngc 4605 ($R = 4$ Kpc) to Ugc 2885 ($R = 122$ Kpc)*. Astrophysical Journal, 1980. **238**(2): p. 471-&.
3. Tully, R.B. and J.R. Fisher, *New Method of Determining Distances to Galaxies*. Astronomy & Astrophysics, 1977. **54**(3): p. 661-673.
4. Faber, S.M. and R.E. Jackson, *Velocity Dispersions and Mass-to-Light Ratios for Elliptical Galaxies*. Astrophysical Journal, 1976. **204**(3): p. 668-683.
5. Milgrom, M., *A Modification of the Newtonian Dynamics as a Possible Alternative to the Hidden Mass Hypothesis*. Astrophysical Journal, 1983. **270**(2): p. 365-370.
6. Sanders, R.H., *A stratified framework for scalar-tensor theories of modified dynamics*. Astrophysical Journal, 1997. **480**(2): p. 492-502.
7. Bekenstein, J.D., *Relativistic gravitation theory for the modified Newtonian dynamics paradigm*. Physical Review D, 2004. **70**(8).
8. McGaugh, S.S. and W.J.G. de Blok, *Testing the dark matter hypothesis with low surface brightness galaxies and other evidence*. Astrophysical Journal, 1998. **499**(1): p. 41-65.
9. McGaugh, S.S., et al., *The baryonic Tully-Fisher relation*. Astrophysical Journal, 2000. **533**(2): p. L99-L102.
10. Lelli, F., et al., *The baryonic Tully-Fisher relation for different velocity definitions and implications for galaxy angular momentum*. Monthly Notices of the Royal Astronomical Society, 2019. **484**(3): p. 3267-3278.
11. Taylor, G.I., *Statistical theory of turbulence Part 1-4*. Proceedings of the royal society A, 1935. **151**: p. 421.
12. Taylor, G.I., *Production and dissipation of vorticity in a turbulent fluid*. Proceedings of the Royal Society of London Series a-Mathematical and Physical Sciences, 1938. **164**(A916): p. 0015-0023.
13. de Karman, T. and L. Howarth, *On the statistical theory of isotropic turbulence*. Proceedings of the Royal Society of London Series a-Mathematical and Physical Sciences, 1938. **164**(A917): p. 0192-0215.
14. Batchelor, G.K., *The Theory of Homogeneous Turbulence*. 1953, Cambridge, UK: Cambridge University Press.
15. Richardson, L.F., *Weather Prediction by Numerical Process*. 1922, Cambridge, UK: Cambridge University Press.
16. Kraichnan, R.H., *Inertial Ranges in 2-Dimensional Turbulence*. Physics of Fluids, 1967. **10**(7): p. 1417-+.
17. Xu, Z., *The maximum entropy distributions of collisionless particle velocity, speed, and energy for statistical mechanics of self-gravitating collisionless flow (SG-CFD)*. arXiv:2110.03126v1 [astro-ph.CO], 2021.
18. Xu, Z., *Inverse mass cascade of self-gravitating collisionless flow and effects on halo deformation, energy, size, and density profiles*. arXiv:2109.12244v1 [astro-ph.CO], 2021.
19. Xu, Z., *Inverse mass cascade of self-gravitating collisionless flow and effects on halo mass functions*. arXiv:2109.09985v1 [astro-ph.CO], 2021.
20. Xu, Z., *Inverse and direct cascade of kinetic and potential energy for self-gravitating collisionless dark matter flow and effects of halo shape on energy cascade*. arXiv:2110.13885v1 [astro-ph.GA], 2021.

21. Xu, Z., *The evolution of baryonic-to-halo mass relation from mass and energy cascade in dark matter flow*. arXiv:, 2022.
22. Xu, Z., *The two-thirds law for pairwise velocity and origin of critical MOND acceleration from distributions of density, velocity, and acceleration in dark matter flow*. arXiv:2202.06515, 2022.
23. Xu, Z., *Postulating dark matter particle mass and properties from two-thirds law for self-gravitating collisionless flow*. arXiv:2202.07240v1, 2022.
24. Xu, Z., *The statistical theory of self-gravitating collisionless dark matter flow and the correlation, structure, and dispersion functions for velocity, density, and potential fields*. arXiv:2202.00910 [astro-ph.CO], 2022.
25. Xu, Z., *The statistical theory of self-gravitating collisionless dark matter flow and high order kinematic and dynamic relations for velocity correlations on small and large scales*. arXiv:2202.02991 [astro-ph.CO], 2022.
26. Xu, Z., *The mean flow, velocity dispersion, and evolution of rotating and growing dark matter halos and their effects on the energy transfer in self-gravitating collisionless flow*. arXiv:2201.12665 [astro-ph.GA], 2022.
27. Mo, H., F. van den Bosch, and S. White, *Galaxy formation and evolution*. 2010, Cambridge: Cambridge University Press.
28. Peebles, P.J.E., *The Large-Scale Structure of the Universe*. 1980, Princeton, NJ: Princeton University Press.
29. C. S. Frenk, et al., *Public Release of N-body simulation and related data by the Virgo consortium*. arXiv:astro-ph/0007362v1 2000.
30. Jenkins, A., et al., *Evolution of structure in cold dark matter universes*. Astrophysical Journal, 1998. **499**(1): p. 20.
31. Colberg, J.M., et al., *Linking cluster formation to large-scale structure*. Monthly Notices of the Royal Astronomical Society, 1999. **308**(3): p. 593-598.
32. Sheth, R.K., H.J. Mo, and G. Tormen, *Ellipsoidal collapse and an improved model for the number and spatial distribution of dark matter haloes*. Monthly Notices of the Royal Astronomical Society, 2001. **323**(1): p. 1-12.
33. Irvine, W.M., *Local Irregularities in a Universe Satisfying the Cosmological Principle*. 1961, HARVARD UNIVERSITY.
34. Layzer, D., *A Preface to Cosmogony. I. The Energy Equation and the Virial Theorem for Cosmic Distributions*. Astrophysical Journal, 1963. **138**: p. 174.
35. Xu, Z., *The evolution of energy, momentum, and spin parameter in self-gravitating collisionless dark matter flow and integral constants on large and small scales*. arXiv:2202.04054 [astro-ph.CO], 2022.
36. Xu, Z., *A non-radial two-body collapse model (TBCM) for gravitational collapse of dark matter in expanding background and generalized stable clustering hypothesis (GSCP)*. arXiv:2110.05784v1 [astro-ph.CO], 2021.
37. Xu, Z., *Mass functions of dark matter halos from maximum entropy distributions for self-gravitating collisionless flow*. arXiv:2110.09676v1 [astro-ph.CO], 2021.
38. Dai, D.C. and C.Y. Lu, *Can the Lambda CDM model reproduce MOND-like behavior?* Physical Review D, 2017. **96**(12).
39. Milgrom, M., *High-redshift rotation curves and MOND*. arXiv:1703.06110 2017.
40. Milgrom, M., *MOND - A pedagogical review*. Acta Physica Polonica B, 2001. **32**(11): p. 3613-3627.